AIAA SciTech Forum
23-27 January 2023, National Harbor, MD & Online
AIAA SCITECH 2023 Forum

10.2514/6.2023-2639

On-Board Optimal Feedback Controller Generation for Hypersonic Re-Target Scenarios

Mihir Vedantam*[1], Carlos Vargas Venegas †[2], Damien Guého‡[2], Puneet Singla§[2], and Maruthi R. Akella¶[1]
[1]*The University of Texas at Austin, Austin, TX, 78712*
[2]*The Pennsylvania State University, University Park, PA, 16802*

This paper presents a framework for rapid onboard generation of hypersonic trajectories. We specifically focus on the hypersonic re-target scenario, which occurs when a vehicle is launched with a nominal target and corresponding optimal trajectory, but receives a new terminal target after the vehicle has already flown part of the nominal trajectory. Qualitatively speaking, we present a novel blend of data-driven learning approaches with indirect optimal control techniques involving banks of open-loop trajectories. The learning is accomplished using sparse approximation techniques resulting in a numerically parsimonious surface fit that is well-suited for onboard computations. As part of the re-targeting mission, the vehicle uses this surface fit to generate optimal feedback controllers in real-time. We demonstrate the application of our proposed framework for planar hypersonic missions with re-targeting.

I. Introduction

Hyperosnic trajectory guidance and control has become an active research area in recent years. The highly nonlinear nature of the flight dynamics, the uncertainty associated with the launch and target conditions, and stringent constraints upon state and control variables make fast on-board computation of hypersonic trajectories a major technical challenge. With a few exceptions, the solution to these trajectory guidance problems is found offline using ground-based computers and requires significant computation with operator interference. In such traditional settings, one seeks to generate a large number of optimal trajectories offline that can subsequently be utilized online to rapidly generate trajectories via interpolation [1, 2] and/or data-driven approaches [3, 4]. Individual trajectories are generated using well-studied optimal control techniques. One approach is using powerful off-the-shelf direct optimizers to solve the problem [5–10]. The application of indirect optimal control theory [11] in conjunction with continuation methods [12] has also been demonstrated to be highly effective for computation of optimal hypersonic trajectories [13–16, 16, 17]. Due to the fact that indirect schemes often result in computationally challenging two-point boundary value problems,

*Graduate Student, Department of Aerospace Engineering and Engineering Mechanics, vedantam.mihir@utexas.edu.
†Graduate Student, Department of Aerospace Engineering, AIAA Student Member, cvv5110@psu.edu.
‡Graduate Student, Department of Aerospace Engineering, AIAA Student Member, AAS Student Member, djg76@psu.edu.
§Professor, Department of Aerospace Engineering, AIAA Associate Fellow, AAS Fellow, psingla@psu.edu.
¶Ashley H. Priddy Centennial Professor, Department of Aerospace Engineering and Engineering Mechanics, AIAA Fellow, AAS Fellow, makella@mail.utexas.edu.

the judicious integration of numerical stabilization schemes within the continuation process [18, 19] has delivered significant robustness alongside convergence guarantees for hypersonic trajectory optimization problems [20, 21].

Despite these significant advances in hypersonic trajectory guidance, one particular aspect that remains highly challenging and has received relatively limited attention in the open literature is the online/onboard re-targeting problem. To further illustrate this scenario, often, the vehicle launch state and the target conditions are uncertain. In such settings, the vehicle is "pre-loaded" with a placeholder nominal trajectory toward the expected target location that will need to be updated online whenever new information is received. Another scenario to consider is when the terminal target is changed part-way through the trajectory as in the case for many-on-many hypersonic engagement settings. These re-targeting trajectory generation problems require fast on-board computation, i.e., speed, memory usage, and numerical robustness.

The major contribution of this paper is that we propose sparse collocations that deliver optimal feedback controllers for real-time for hypersonic re-targeting maneuvers. Sparse collocation methods [22–25] use parsimonious representations to derive optimal feedback control laws that remain valid inside the prescribed domain of uncertainty quantified through initial condition dispersions, final/target states, and model parameters (such as due to aerodynamics). The sparse collocation methods make use of non-product quadrature method known as *Conjugate Unscented Transformation* (CUT) [26] for uncertainty quantification in conjunction with sparse approximation methods to derive optimal feedback control law from minimal number of open-loop solutions [23–25]. The CUT method is used to optimally sample the prescribed uncertainty domain for initial condition, final conditions and model parameters. An open-loop control problem is solved to generate optimal control profile, cost-to-go (i.e., value function) and co-state value for each of the CUT generated samples. A polynomial approximation for the cost-to-go function in terms of state variables is considered and iterative ℓ_1 optimization problem is solved at each time to choose a sparse polynomial approximation that exactly reproduce value function and co-state values for each CUT provided samples. Hence, a feedback structure for the cost-to-go function and thus feedback controller is derived from minimal number of optimal-loop solutions.

Central to the approach we take in this paper is the uncertainty quantification that efficiently samples the mission parameter space and thus, reduces the number of trajectories that need to be computed offline. We then use stabilized continuation to produce all the required nominal trajectories. Next, we exploit the recent advances in sparse approximation to generate a parsimonious model which provides optimal feedback controllers as a function of mission variables. Finally, we generate a validation set of re-target trajectories to compare the optimal feedback controller model to the offline generated trajectories.

The rest of this paper is organized as follows: Section II contains a more detailed description of the hypersonic re-target problem and the corresponding dynamics. Section III details out our proposed methodology and any background information that is needed. Section IV shows the preliminary results we have achieved with our methodology. Finally, Section V contains any concluding remarks and plans for the final version of this paper.

II. Problem Statement

This section contains a more detailed description of the hypersonic re-targeting problem. It is salient to note that the dynamics and cost functional are generalized in this section, because our proposed methodology is agnostic to the specifics of the problem. First, we start with high-level description of the optimal hypersonic trajectory generation problem given by,

$$\text{Minimize} : J = K(\mathbf{x}(t_f), t_f) + \int_{t_0}^{t_f} \mathcal{L}(\boldsymbol{x}, \boldsymbol{u}, t) dt \tag{1a}$$

$$\text{Subject to} : \dot{x} = \boldsymbol{f}(\mathbf{x}, \mathbf{u}, t), \tag{1b}$$

$$\Upsilon(\mathbf{x}(t_0), t_0) = 0, \tag{1c}$$

$$\Psi(\mathbf{x}(t_f), t_f) = 0 \tag{1d}$$

wherein $K(\boldsymbol{x}(t_f), t_f)$ is the cost associated with the terminal conditions and $\mathcal{L}(\boldsymbol{x}, \boldsymbol{u}, t)$ is the running cost over the entire trajectory. The dynamics are represented by $\boldsymbol{f}(\mathbf{x}, \mathbf{u}, t)$, $\Upsilon(\mathbf{x}(t_0), t_0)$ is the collection of constraints associated with the initial conditions and $\Psi(\mathbf{x}(t_f), t_f)$ is the collection of constraints associated with the terminal conditions.

The hypersonic re-target problem, on the other hand, has a similar mathematical representation as in Eq. 1, but at some point along the nominal optimal trajectory corresponding to $t = t_i$, the optimal control problem is updated:

$$\text{Minimize} : J = K(\mathbf{x}(t_f), t_f) + \int_{t_i}^{t_f} \mathcal{L}(\boldsymbol{x}, \boldsymbol{u}, t) dt \tag{2a}$$

$$\text{Subject to} : \dot{x} = \boldsymbol{f}(\mathbf{x}, \mathbf{u}, t), \tag{2b}$$

$$\Upsilon_n(\mathbf{x}(t_i), t_i) = 0, \tag{2c}$$

$$\Psi_n(\mathbf{x}(t_f), t_f) = 0 \tag{2d}$$

wherein the n subscript corresponds to the n-th retargeting update for the hypersonic trajectory. The updated initial constraints, $\Upsilon_n(\mathbf{x}(t_i), t_i)$ will be the vehicle states at the time $t = t_i$ when the target conditions are updated. The controls can be included in the initial constraints as well to maintain control continuity over the entire trajectory, especially at the time instants where the retargeting is commanded. In this study, the control constraints are not included, so the solution will have a jump discontinuity in the controls at the re-target point. Finally, the terminal constraints, $\Psi_n(\mathbf{x}(t_f), t_f)$, are the updated re-targeted points. A representational view for a re-targeting scenario is depicted in Fig. 1.

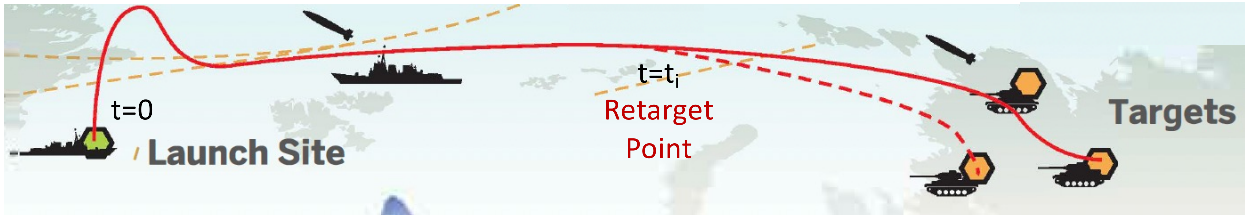

Figure 1 Illustration of a Re-Target Scenario

III. Technical Approach

A top-level overview of our proposed technical approach is shown in Fig. 2. Qualitatively speaking, the proposed methodology involves sampling the prescribed uncertainty domain for initial condition, final conditions and model parameters. Then, an open-loop solution is calculated for each CUT point at each time step, along the nominal trajectory. The free variable, time of flight (t_f), is expanded as a polynomial expansion (using basis functions $\mathbf{\Phi}(x)$) and a sparse approximation problem is posed as an ℓ_1 optimization problem to solve for the minimum number of coefficients, $\boldsymbol{c}^*(t)$, to explain the data. We denote $\mathbf{\Omega}(x_0)$ to represent the domain of unknown but bounded variables, $\mathbf{\Phi}(x)$ are the basis functions used in the approximation, $\boldsymbol{c}^*(t)$ are the coefficients that correspond to the basis functions. $\boldsymbol{x}$ represents the states, $\boldsymbol{\nu}$ are the Lagrange multipliers corresponding to the terminal conditions and $\boldsymbol{\lambda}$ are the Lagrange multipliers corresponding to the dynamics. The major challenge lies in finding a parsimonious representation for the control variables as a function of mission variables and learning this surface from as few simulations as possible, i.e., minimize the amount of training dataset. To achieve this objective, we make use of advances in sparse approximation in conjunction with optimal sampling method known as CUT. The CUT methodology curtails the curse of dimensionality associated with sampling a multi-dimension space, while the sparse approximation method allows us to choose a subset of basis functions from an overcomplete dictionary to parametrize the control variables accurately over the prescribed domain, Ω. The three blocks in the middle of the diagram showcase the general workflow of the proposed methodology, and they are explained in more detail in the following two subsections.

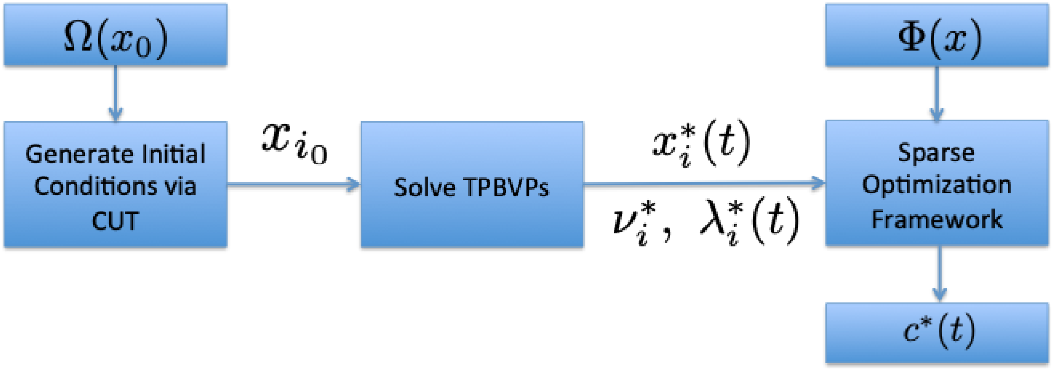
$\Omega(x_0)$
Generate Initial Conditions via CUT
x_{i_0}
Solve TPBVPs
$x_i^*(t)$
$\nu_i^*,\ \lambda_i^*(t)$
$\Phi(x)$
Sparse Optimization Framework
$c^*(t)$

Figure 2 Schematic Representation of the Proposed Methodology

A. Solving Two Point Boundary Value Problems (TPBVPs)

Because the Lagrange multipliers corresponding to the vehicle dynamics and terminal condition constraints are required for the sparse approximation framework, the open-loop trajectories must be produced using indirect optimal control. Any two point boundary value problem solver can be used in this step; however, we use the stabilized continuation method to find the open-loop trajectories corresponding to each CUT point. Specifically, after the application of the Euler-Lagrange first-order conditions of optimality to the optimal control problem defined in Eq. 1, we get a fully determined root-solving problem of the form,

$$F(\mathbf{z}) = 0 \tag{3}$$

wherein z is a collection of the unknown variables associated with the TPBVP. We can artificially embed a continuation parameter, $s \in [0\ 1]$, into the root solving function as $\mathbf{F}(s, \mathbf{z}) = 0$. In the case of the hypersonic re-target problem, the dependence of the nonlinear root solving problem on the continuation parameter, s, is implicit. We can then apply the stabilized continuation method [18–21],

$$\frac{\mathrm{d}\mathbf{z}}{\mathrm{d}s} = \left[\frac{\partial \mathbf{F}}{\partial \mathbf{z}}\right]^{-1} \left[A_m \mathbf{F}(\mathbf{z}, s) + \boldsymbol{\nu}_s - \frac{\partial \mathbf{F}}{\partial s}\right],\ s \in [0, 1],\ \mathbf{z}(s_0) \text{ given} \tag{4}$$

wherein A_m is a user-selected Hurwitz matrix that attenuates any error introduced in the continuation procedure due to either a “bad” initial guess or numerical error accumulated along the continuation interval. If the stabilizing input, ν_s, is selected to be the linear time-invariant system minimum effort control law, then any error introduced by a “bad” initial guess is completely attenuated over the continuation interval and a perfect solution is returned.

B. Solving Two-Point Boundary Value Problems via Hamilton-Jacobi Bellman Equation

The optimal control law that solves a given TPBVP is directly related to the value function J that satisfies the Hamilton-Jacobi-Bellman (HJB) equation, which is a nonlinear, hyperbolic partial differential equation over a domain of interest. A feedback control law may be identified by solving the HJB equation, which is necessary and sufficient for optimality [23, 24], and enables access to the costates for any given input $\mathbf{x}$ via partial differentiation,

$$\lambda_{x_i} = \frac{\partial J(\mathbf{x})}{\partial x_i} \tag{5}$$

As no closed-form analytical solution exists to the HJB equation, the principal objective of the proposed methodology is to find an accurate approximation to the optimal return function given only a finite set of open-loop trajectories obtained from the stabilized continuation method. Once such a function approximation has been identified, the optimal control law may be computed via the stationarity condition in the necessary conditions for optimality,

$$\frac{\partial \mathcal{H}}{\partial u} = 0 \tag{6}$$

The costates that appear in the representation of the optimal control as a function of states and costates may be determined using Eqs. (5) once the optimal return function approximation has been obtained. The following section details the optimization framework adopted to determine a parsimonious approximation to the optimal return function.

C. Sparse Optimization Framework

Let us consider a scalar function f with known values at some prescribed collocation points $\boldsymbol{x}_i$, $i = 1, 2, \cdots, N$ at each time step t_k. Considering a set of basis functions $\{\phi_i\}_{i=1\ldots\infty}$, $\phi_i : \mathbb{R}^n \to \mathbb{R}$, f can be approximated as a linear combination of these basis function such that $\forall\, \boldsymbol{x} \in \mathbb{R}^n$,

$$f(\boldsymbol{x}) = \sum_{i=1}^{\infty} c_i \phi_i(\boldsymbol{x}), \tag{7}$$

where $\{c_i\}_{i=1..\infty}$, is a set of unknown coefficients. It is desired to choose the basis functions which allow representing f in Eq. (7) with as few terms as possible. In this respect, the summation in Eq. (7) is taken over a finite number of m basis functions and approximated as:

$$f(\boldsymbol{x}) \simeq \sum_{i=1}^{m} c_i \phi_i(\boldsymbol{x}) = \boldsymbol{c}^T \boldsymbol{\phi}(\boldsymbol{x}), \tag{8}$$

where $\boldsymbol{c}, \boldsymbol{\phi}(\boldsymbol{x}) \in \mathbb{R}^m$ are the unknown coefficient and known basis functions vectors. One can find an optimal value of the coefficient vector $\boldsymbol{C}$ by solving the weighted two-norm minimization problem:

$$\boldsymbol{c}^* = \min_{\boldsymbol{c}} \frac{1}{2}\boldsymbol{e}^T R \boldsymbol{e}, \tag{9}$$

with $\boldsymbol{e} = \boldsymbol{f} - \boldsymbol{\Phi c}$ is the error to minimize in the 2-norm sense, $\boldsymbol{f} = \begin{bmatrix} f(\boldsymbol{x_1}) & f(\boldsymbol{x_2}) & \cdots & f(\boldsymbol{x_N}) \end{bmatrix}^T \in \mathbb{R}^N$ is the vector composed of the scalar function evaluated at the collocation points and $\boldsymbol{\Phi} = \begin{bmatrix} \boldsymbol{\phi}(\boldsymbol{x_1}) & \boldsymbol{\phi}(\boldsymbol{x_2}) & \cdots & \boldsymbol{\phi}(\boldsymbol{x_N}) \end{bmatrix} \in \mathbb{R}^{m \times N}$ is the matrix of all the basis functions evaluated at the collocation points. The weight matrix $R \in \mathbb{R}^{N \times N}$ can be chosen appropriately depending upon the noise in the measurement data. Depending upon the size of N and m, the aforementioned optimization problem can be over-determined or under-determined. In both the cases, one can find the solution with an appropriate pseudo inverse of $\boldsymbol{\Phi}$, i.e.,

$$\boldsymbol{c}^* = \boldsymbol{\Phi}^\dagger \boldsymbol{f} \tag{10}$$

where the superscript * stands for the least-squares solution and the superscript † stands for the pseudo-inverse and its expression depends on the problem:

$$N > m \qquad \text{over-determined} \qquad \boldsymbol{\Phi}^\dagger = \left(\boldsymbol{\Phi}^T R \boldsymbol{\Phi}\right)^{-1} \boldsymbol{\Phi}^T R, \tag{11}$$

$$N < m \qquad \text{under-determined} \qquad \boldsymbol{\Phi}^\dagger = \boldsymbol{\Phi}^T R \left(\boldsymbol{\Phi} R \boldsymbol{\Phi}^T\right)^{-1}, \tag{12}$$

$$N = m \qquad \text{exact solution} \qquad \boldsymbol{\Phi}^\dagger = \boldsymbol{\Phi}^{-1}. \tag{13}$$

We note that Eq. (9) is a minimization problem obtained by choosing some certain collocation points. When one chooses the basis function ϕ_i to be the Lagrange interpolation polynomials, the collocation points are intrinsically defined such that $\phi_i(\boldsymbol{x}_i) = 1$. Although Lagrange interpolation polynomials provide minimal order interpolation functions in a one-dimensional space, this property ceases in multi-dimensional spaces [22]. Furthermore, the number of collocation points and polynomial basis functions would not be the same for a general n-dimensional system. When $N > m$, i.e., the number of collocation points is greater than the number of basis functions and the over-determined system typically does not guarantee an exact solution to the underlying system of equations and hence, should be avoided. An alternative approach is to have $N < m$, i.e., fewer collocation points than the number of basis functions. In our previous work [22–25], it is shown that choosing the collocation points to be CUT points is guaranteed to lead to an under-determined system. This is due to the fact that the growth of CUT points is slower than the equivalent Gaussian quadrature points as well as combinatorial growth of the basis functions.

The variable $\boldsymbol{c}^*$ corresponds to the optimal solution in terms of minimizing the two-norm of the error between the function evaluated at the collocation points and the expansion using known basis functions. Since the two-norm solution is known to pick all the basis functions in the dictionary (especially in the case of noise corrupted measurements), this can lead to a non-parsimonious model and affect on-board computations, especially during the terminal phase of a hypersonic vehicle. In order to reduce the number of basis functions needed to best represents the given set of data and to enforce sparsity, an ideal ℓ_0 norm of the coefficient vector $\boldsymbol{c}$ needs to be minimized subject to the constraints of Eq. (8). The ℓ_0 norm corresponds to the cardinality of the coefficient vector and its minimization leads to a non-convex problem. However, the ℓ_0 norm minimization problem can be approximated by an iterative ℓ_1 norm minimization problem which is convex in nature with a guaranteed solution [27]:

$$\boldsymbol{c}^\star = \min_{\boldsymbol{c}^p} ||W^p \boldsymbol{c}^p||_1 \tag{14}$$

$$\text{such that} \quad ||\boldsymbol{f} - \boldsymbol{\Phi}\boldsymbol{c}^p||_2 \leq \varepsilon \, ||\boldsymbol{f} - \boldsymbol{\Phi}\boldsymbol{c}^*||_2 \, , \quad \varepsilon \geq 1 \tag{15}$$

where p is the iteration, $\boldsymbol{c}^p$ is the optimization variable at iteration p, $\boldsymbol{f}$ and $\boldsymbol{\Phi}$ are defined as before and $\boldsymbol{c}^*$ is the optimal two-norm solution. Notice that two-norm constraint of Eq. (15) corresponds to the satisfaction of Eq. (8). Rather than using the equality constraint of Eq. (8) a two-norm error is bounded by the optimal pseudo-norm solution with ε being the user-defined relaxation on the two-norm error. This allows one to tradeoff sparsity with approximation error. Furthermore, W^p is a diagonal matrix containing a known weight w_i for the i^{th} optimization variable. Initially, w_i can be chosen based upon any a-priori knowledge about the structure of f, the form of the least-squares solution or can simply be chosen to be one. In the subsequent iterations, the value of w_i is adapted according to the following formula to penalize the coefficients that are smaller than a predefined threshold δ:

$$w_i^p = \frac{1}{\left|c_i^{p-1}\right| + \eta}, \; 1 \leq i \leq m \tag{16}$$

and η is a small positive number to avoid division by zero. This iterative procedure is repeated unless the computed coefficients converged within a prescribed tolerance. The solution of this iterative ℓ_1 minimization problem provides a subset of basis functions which plays a dominant role in explaining f. Finally, an optimal pseudo-inverse solution for the coefficients is obtained for only these subset of basis functions.

D. Summary of Proposed Methodology

The main steps of the proposed algorithm for the creation of the feedback controller can be enumerated as follows:

1) Generate the N CUT points in the domain of interest for the free variables at initial and final times.
2) Solve N open-loop optimal control problems for each CUT point using the continuation method.

3) Approximate the variables of interest by a truncated sum of basis functions multiplied by unknown coefficients as in Eq. (8).
4) Solve the weighted two-norm and the ℓ_1 norm optimization problems of Eqs. (9) and (14)-(15) to find the unknown coefficients for the non-parsimonious and parsimonious models for the variables of interest.
5) Define the feedback controller by utilizing the closed-form function approximations obtained in the previous step.

IV. Application Results

We have a representative set of results that showcase the major features of our approach in this extended abstract version of the paper. These results cover a variety of single-target and multiple re-targeting engagement scenarios for a rigid hypersonic vehicle in planar motion.

A. Planar Hypersonic Dynamics

The geocentric planar hypersonic dynamics are as follows,

$$\begin{aligned}
\dot{h} &= v \sin\gamma \\
\dot{\theta} &= \frac{v\cos\gamma}{r} \\
\dot{v} &= \frac{-D}{m} - \frac{\mu\sin\gamma}{r^2} \\
\dot{\gamma} &= \frac{L}{mv} + \left(\frac{v}{r} - \frac{\mu}{vr^2}\right)\cos\gamma
\end{aligned} \tag{17}$$

In Eq. 17, h is the altitude of the vehicle, θ is the downrange (i.e. degrees traveled in plane from the vehicle's initial latitude), v is the vehicle velocity and γ is the flight path angle. The control input appears explicitly in the lift, L, and drag, D, terms as follows,

$$\begin{aligned}
C_D &= C_{D_{\alpha^2}}\alpha^2 + C_{D_0} \\
C_L &= C_{L_\alpha}\alpha \\
D &= \frac{1}{2}\rho v^2 C_D A_{\text{ref}} \\
L &= \frac{1}{2}\rho v^2 C_L A_{\text{ref}}
\end{aligned} \tag{18}$$

The atmospheric density is drawn from an exponential model as

$$\rho = \rho_0 \exp\left(-\frac{h}{H}\right) \tag{19}$$

Radial distance for a spherical earth, r, is measured as the sum of Earth's radius, r_e, and altitude, h,

$$r = r_e + h \tag{20}$$

The rest of the variables are vehicle and environmental parameters which are documented in Table 1.

Table 1 Vehicle and environment parameters.

Parameter	Symbol	Value
Surface air density	ρ_0	$1.2\ \mathrm{kg/m^3}$
Vehicle reference area	A_{ref}	$0.2919\ \mathrm{m^2}$
Gravitational constant	μ	$3.986 * 10^{14}\ \mathrm{m^3/s^2}$
Mass	m	340.1943 kg
Scale height	H	7500 m
Radius of Earth	r_e	6378000 m

The cost functional for the optimal control problem is maximum speed upon impact, given by

$$J = -v^2(t_f) \tag{21}$$

Finally, the nominal initial and terminal conditions used for this study are shown in Table 2.

Table 2 Initial and terminal constraints

Variable	**Deployment** ($t = 0$)	**Impact** ($t = t_f$)
Time, t	0	Free
Altitude, h	$80,000$	0
Velocity magnitude, v	$4,000$m/s	Free
Flight-path angle, γ	0°	Free
Longitude, θ	0°	5°

After the application of the stationarity condition (Eq. 6), the optimal control is shown to be

$$\alpha = \frac{\lambda_\gamma C_{L_1}}{2C_{D_2}\lambda_v v} \tag{22}$$

B. Definition of Problem Uncertainties and Sampling

The results in this study showcase the application of the proposed framework to the conventional planar hypersonic trajectory generation problem with initial and terminal state uncertainties. Three of the initial conditions and one of the terminal conditions are assumed to be uncertain with the following nominal values and standard deviations:

$$h_0 = 80\text{km} \pm 1\text{km} \tag{23}$$

$$\gamma_0 = 0° \pm 1° \tag{24}$$

$$\theta_0 = 0° \pm 0.1° \tag{25}$$

$$\theta_f = 5° \pm 0.1° \tag{26}$$

The CUT algorithm is used to optimally sample the four-dimensional space defined by Eqs. (23)-(26). The CUT samples are depicted in Figure 3 as spheres and sum up to 161 points. These CUT points define TPBVPs that are solved using the stabilized continuation method introduced in Sec. III.A to obtain the open-loop trajectories. Solving these TPBVPs creates a set of 161 optimal trajectories for the states and costates shown in Figs. 4 and 5. This set of optimal trajectories is termed the *field of extremals*, and is used to construct the optimal feedback controller using the methodology in Sec. III.C.

C. Generation of the Feedback Controller

As detailed in Sec. III.B, the optimal feedback controller is based on an approximation to the optimal return function that satisfies the HJB equation, and the stationarity condition in Eq. (22). The set of basis functions defined in Sec. III.C is used to write the optimal return function approximation as a truncated sum of monomials multiplied by unknown coefficients such that its partial derivatives with respect to the states yield the optimal costates,

$$V(\mathbf{x}) = \sum_{i=1}^{m_V} c_i \phi_i(\mathbf{x}) \tag{27}$$

$$\lambda_h(t) = \sum_{i=1}^{m_V} c_i \frac{\partial \phi_i(\mathbf{x})}{\partial h} \tag{28}$$

$$\lambda_v(t) = \sum_{i=1}^{m_V} c_i \frac{\partial \phi_i(\mathbf{x})}{\partial v} \tag{29}$$

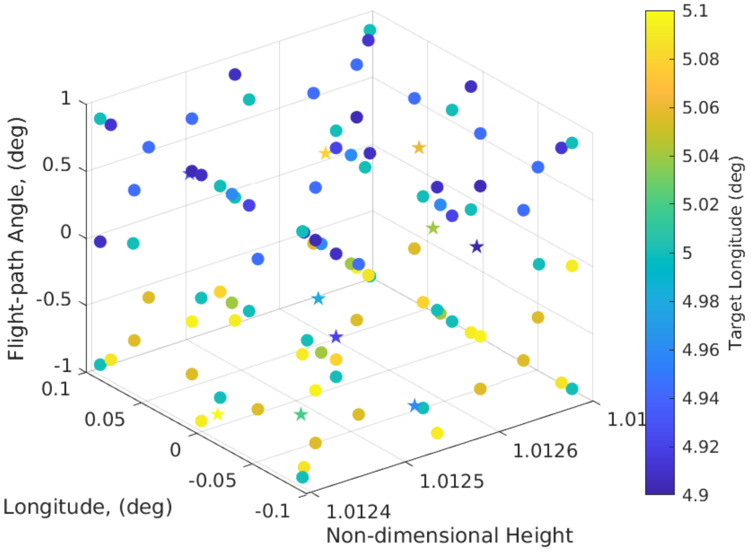

Figure 3 CUT (spheres) and validation (stars) samples.

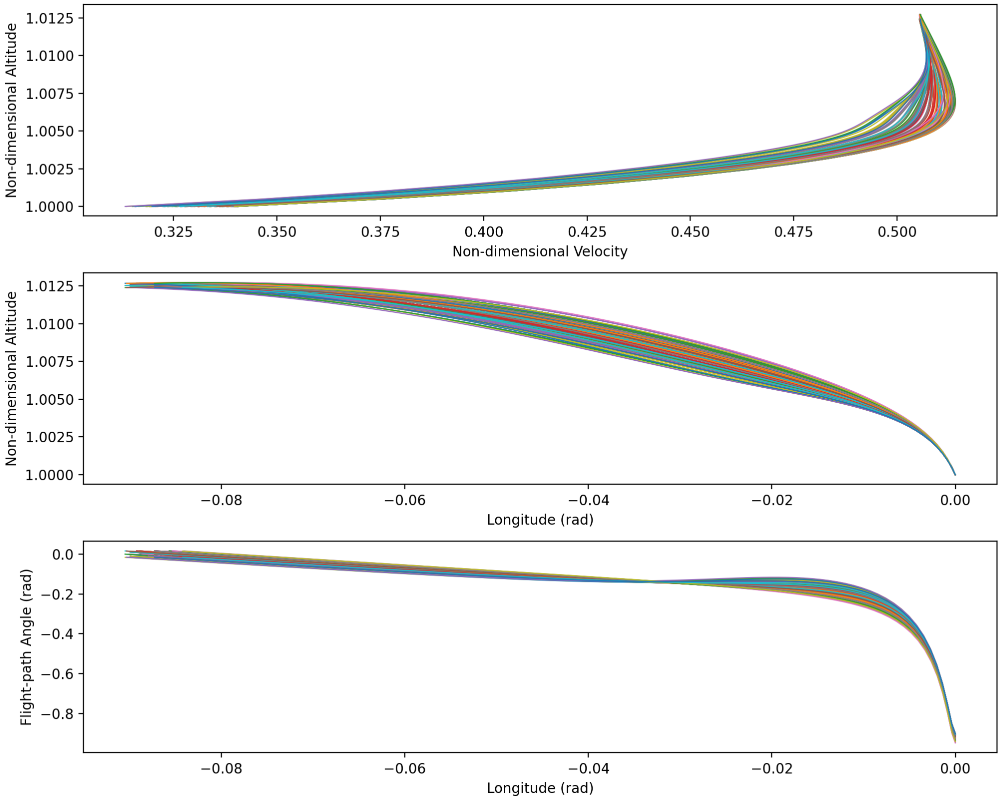

Figure 4 Optimal state trajectories obtained using the continuation method

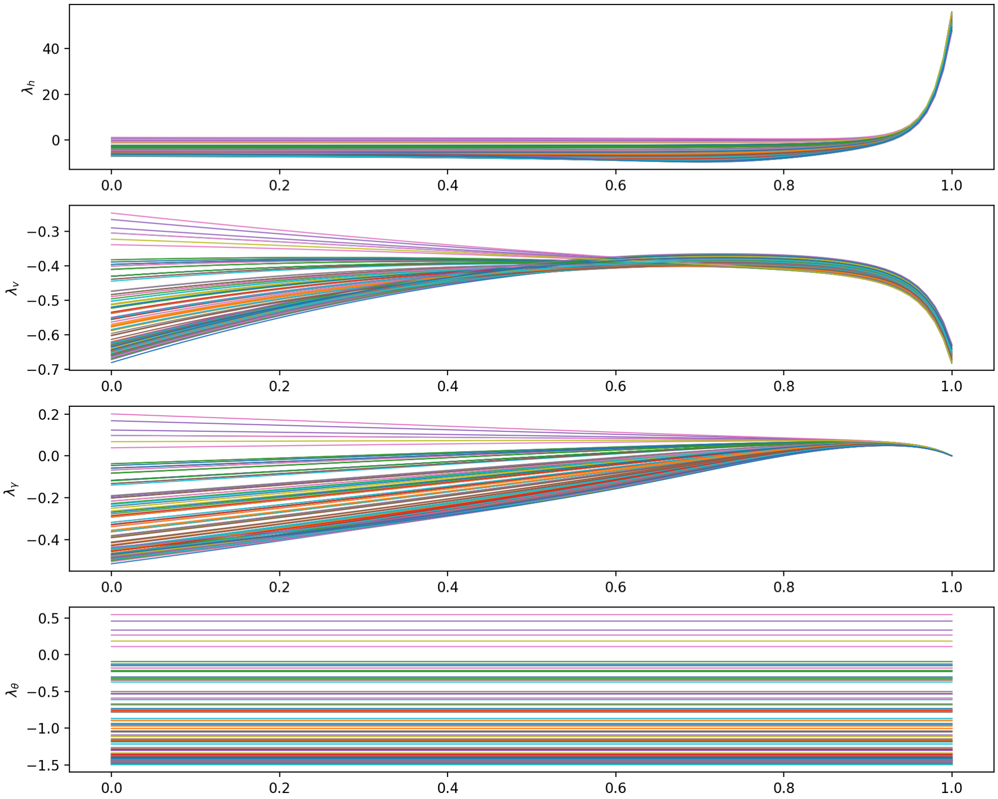

Figure 5 Optimal costate trajectories obtained using the continuation method

$$\lambda_\gamma(t) = \sum_{i=1}^{m_V} c_i \frac{\partial \phi_i(\mathbf{x})}{\partial \gamma} \tag{30}$$

$$\lambda_\theta(t) = \sum_{i=1}^{m_V} c_i \frac{\partial \phi_i(\mathbf{x})}{\partial \theta} \tag{31}$$

The Lagrange multipliers $\nu_h = \lambda_h(t_f)$ and $\nu_\theta = \lambda_\theta(t_f)$ are also expanded as a truncated sum of monomials multiplied by unknown coefficients,

$$\nu_h = \sum_{i=1}^{m_{\nu_h}} a_i \phi_i(\mathbf{x}) \tag{32}$$

$$\nu_\theta = \sum_{i=1}^{m_{\nu_\theta}} b_i \phi_i(\mathbf{x}) \tag{33}$$

Hence, given the CUT points and the corresponding open-loop state and costates trajectories, the sparse optimization framework presented in Sec. III.C is employed to determine the unknown coefficients for both the optimal return function in Eq. (27), and the Lagrange multipliers ν_h and ν_θ in Eq. (32)-Eq. (33). This approach creates three different system of linear equations that are amenable for convex optimization tools such as the CVXPY library [28]; this library enable the identification of a parsimonious model for the optimal return function and Lagrange multipliers.

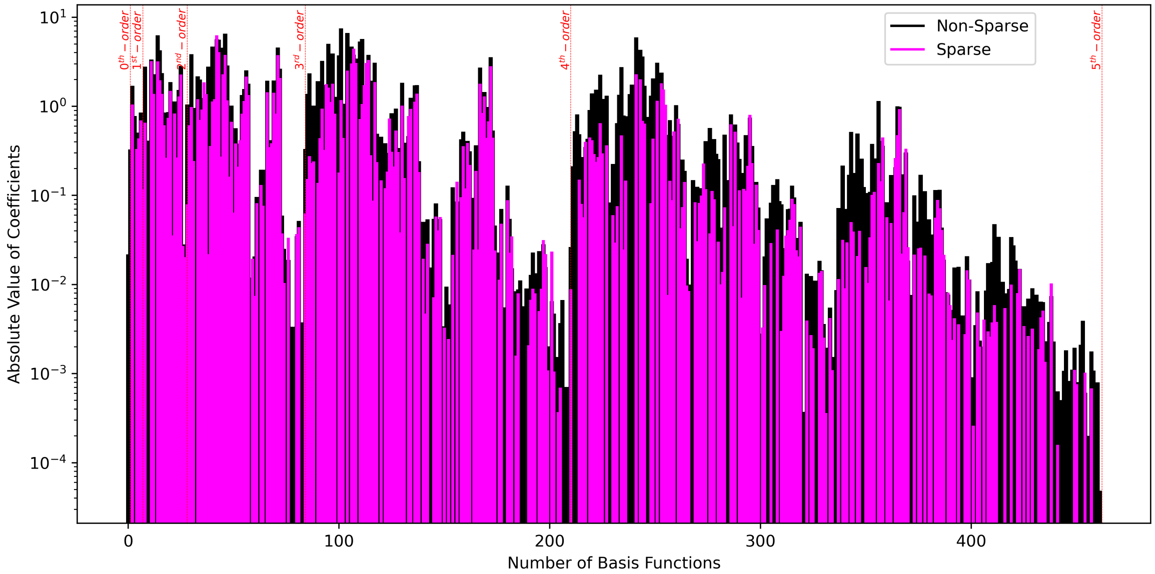

Figure 6 Non-Sparse and Sparse solutions for the coefficients in the optimal return function approximation.

For the optimal return function approximation, the monomials are considered up to 5^{th} order, whereas for the Lagrange multipliers, the monomials are considered up to 9^{th} order. After formulation of the equality constraints, the CVXPY library is utilized to solve the three convex optimization problems, the resulting coefficients for the optimal return function approximation and the Lagrange multipliers are shown in Figs. 6, 7a and7b. For the optimal return function approximation, the least-squares solution finds a set of coefficients for all 462 monomials. The sparse optimization framework filters out unnecessary monomials in the expansion and finds an accurate approximation with 320 active basis functions. Similarly, for the Lagrange multipliers, the least-square solution finds a set of coefficients for all the 2002 monomials. The sparse optimization framework identifies only 266 active basis functions for ν_h, and 316 for the ν_θ. The large magnitude of the coefficients for the Lagrange multipliers relative to optimal return function approximation is attributed to the magnitude of the costates λ_h and λ_θ as shown in Fig. 5.

D. Planar Hypersonic Optimal Trajectory Generation

The optimal feedback controller is now benchmarked against the continuation method in generating optimal solutions for the TPBVP described in Sec. II. Ten different validation trajectories are generated by randomly sampling the initial conditions in Eqs. Eq. (23)-Eq. (25), and selecting terminal longitudes that cover the entirety uncertainty range of the sampling domain. These ten random validation cases are depicted as stars in Fig. 3 and are completely independent of CUT samples.

The results in Figs. 8a and 8b show the state trajectories and control generated by the open-loop and feedback controller solutions for only five validation cases for clarity. The results in these figures show that the feedback controller can accurately reconstruct the optimal control and state trajectories even under the presence of uncertainty in the initial

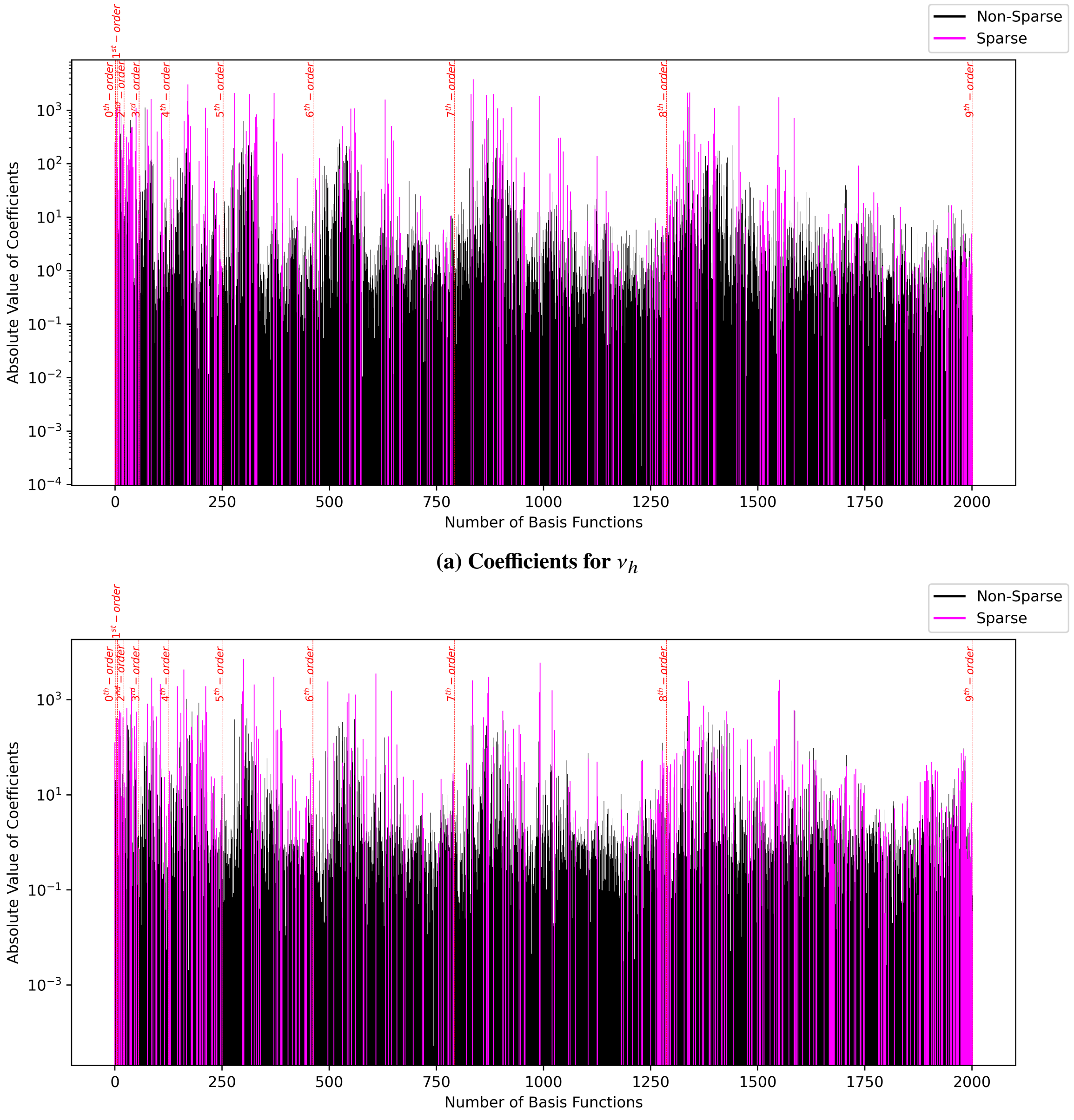

(a) Coefficients for ν_h

(b) Coefficients for ν_θ

Figure 7 Non-sparse and sparse coefficients for the Lagrange multipliers.

and terminal conditions.

An error study is conducted using all ten validation cases for the state, costate, and control solutions from the optimal feedback controller. The mean relative errors of the feedback controller in predicting the Lagrange multipliers ν_h and ν_θ for all ten validation cases are provided in Table 3. The least-squares and sparse solutions perform both with comparable accuracy; this indicates that the sparse optimization algorithm successfully removes unnecessary basis functions from the least-square solution. Now the states, costates, and control solutions from the optimal feedback controller are compared against the open-loop solutions. The root-mean-squared error (RMSE) is calculated for each of the variables of interest over time and averaged among the ten random validation cases. The mean RMSEs are provided in Table 4.

Table 3 Number of basis functions of polynomial series expansions and their accuracy in predicting the costates ν_h and ν_θ.

Variable	Mean Least-squares relative error	Mean sparse relative error	Number of active basis functions
ν_h	1.586×10^{-4}	1.112×10^{-4}	266/2002
ν_θ	6.326×10^{-3}	3.872×10^{-3}	316/2002

Table 4 Accuracy of the feedback controller in reconstructing optimal trajectories for ten different validation cases.

Variable	Mean Least-squares RMSE	Mean Sparse RMSE
Altitude: h	1.129×10^{-5}	1.223×10^{-5}
Velocity: v	5.279×10^{-4}	4.585×10^{-4}
Flight-path Angle: γ	2.429×10^{-4}	1.477×10^{-4}
Longitude: θ	1.126×10^{-5}	1.008×10^{-5}
Costate: λ_v	4.552×10^{-4}	3.522×10^{-4}
Costate: λ_γ	2.122×10^{-4}	1.422×10^{-4}
Optimal Control: u^*	3.341×10^{-3}	2.406×10^{-3}

E. Planar Hypersonic Re-targeting Scenario

Next, the optimal feedback controller is tested for re-targeting scenarios. Two re-targeting scenarios are considered assuming the hypersonic vehicle starts on a nominal trajectory: 1) the re-targeting information arrives once the vehicle

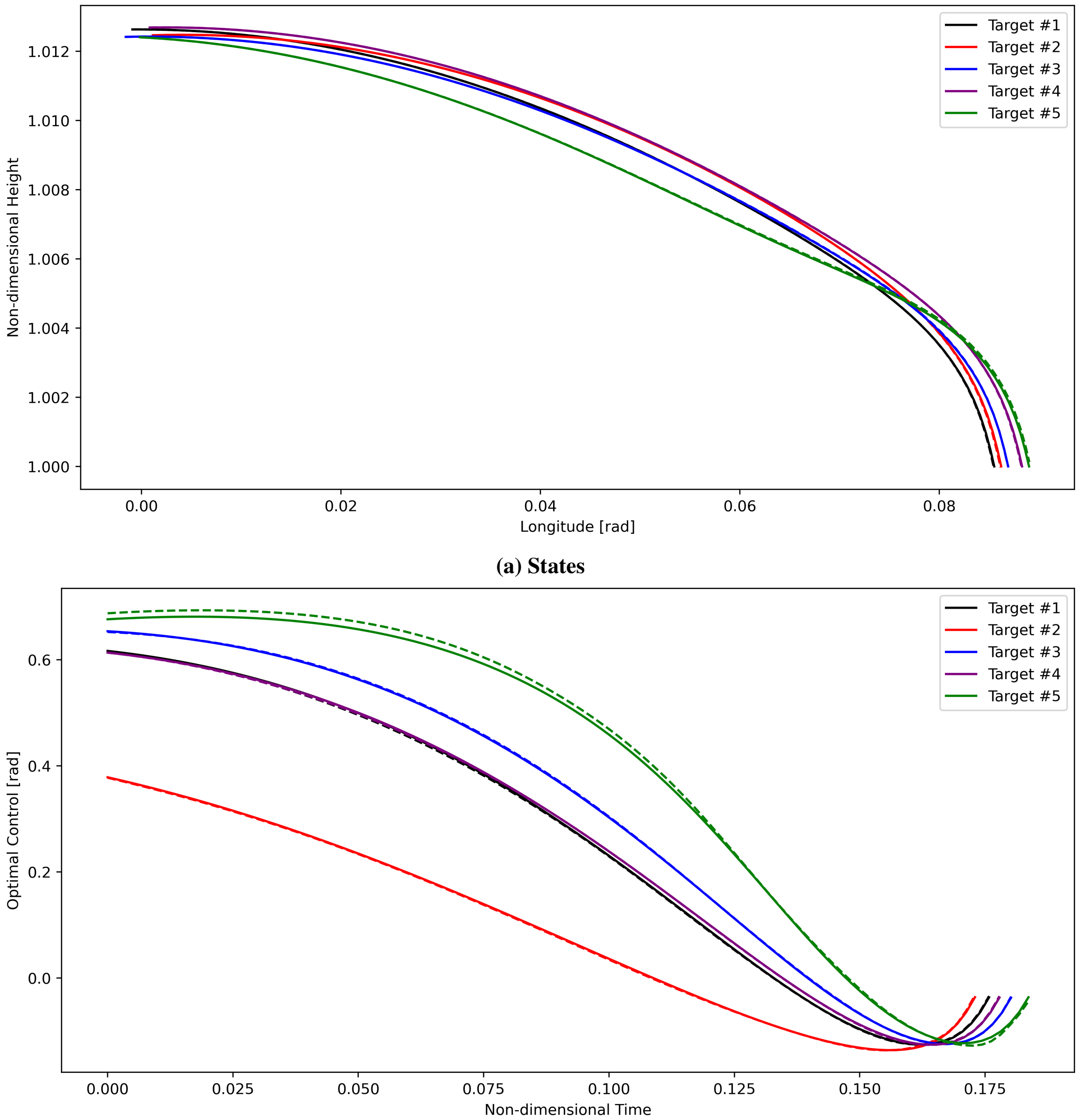

(a) States

(b) Optimal Control

Figure 8 State and optimal control trajectories obtained from the open-loop continuation method and the feedback controller. Solid: open-loop solution. Dashed: feedback controller solution.

is at 20% of its nominal trajectory, and 2) the re-targeting information arrives once the vehicle is at 50% of its nominal trajectory.

First, the re-targeting states and controls at 20% of the nominal trajectory are depicted in Figs. 9a and 9b. At 20% of the nominal trajectory the feedback controller accurately captures the optimal control from the open-loop solution and maintains its accuracy throughout the flight time of the vehicle. The mean RMSE errors among all ten validation cases are reported in Table 5, where both the least-squares and sparse approximations to the optimal return function yield comparable accuracy.

A similar performance is obtained when the re-targeting is considered at 50% of the nominal trajectory as depicted in Figs. 10a and 10b. In accordance with the previous results, the feedback controller accurately captures the optimal control predicted by the open-loop solution throughout the flight time of the vehicle. The mean RMSE errors among all ten validation cases are reported in Table 6.

Table 5 Accuracy of the feedback controller for ten different validation re-target points at 20% of the nominal trajectory.

Variable	**Mean Least-squares RMSE**	**Mean Sparse RMSE**
Altitude: h	9.553×10^{-6}	1.075×10^{-5}
Velocity: v	4.249×10^{-4}	2.801×10^{-4}
Flight-path Angle: γ	2.232×10^{-3}	9.526×10^{-4}
Longitude: θ	8.889×10^{-6}	6.807×10^{-6}
Costate: λ_v	3.039×10^{-3}	3.095×10^{-3}
Costate: λ_γ	8.372×10^{-4}	7.702×10^{-4}
Optimal Control: u^*	1.914×10^{-3}	1.733×10^{-3}

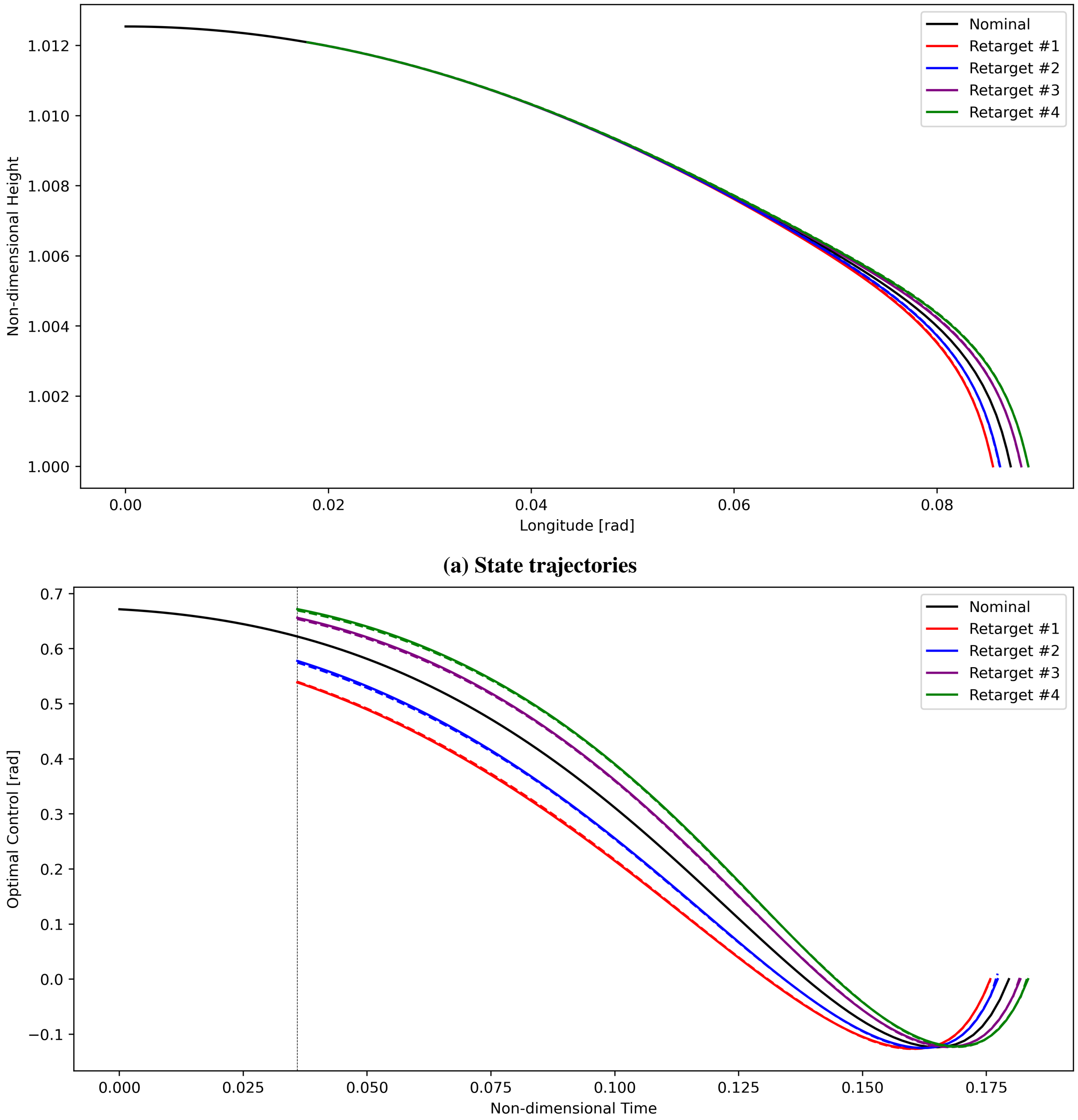

(a) State trajectories

(b) Optimal control trajectories

Figure 9 State and optimal control trajectories obtained from the open-loop continuation method and the feedback controller for the re-targeting scenario at 20% of the nominal trajectory. Solid: open-loop solution. Dashed: feedback controller solution.

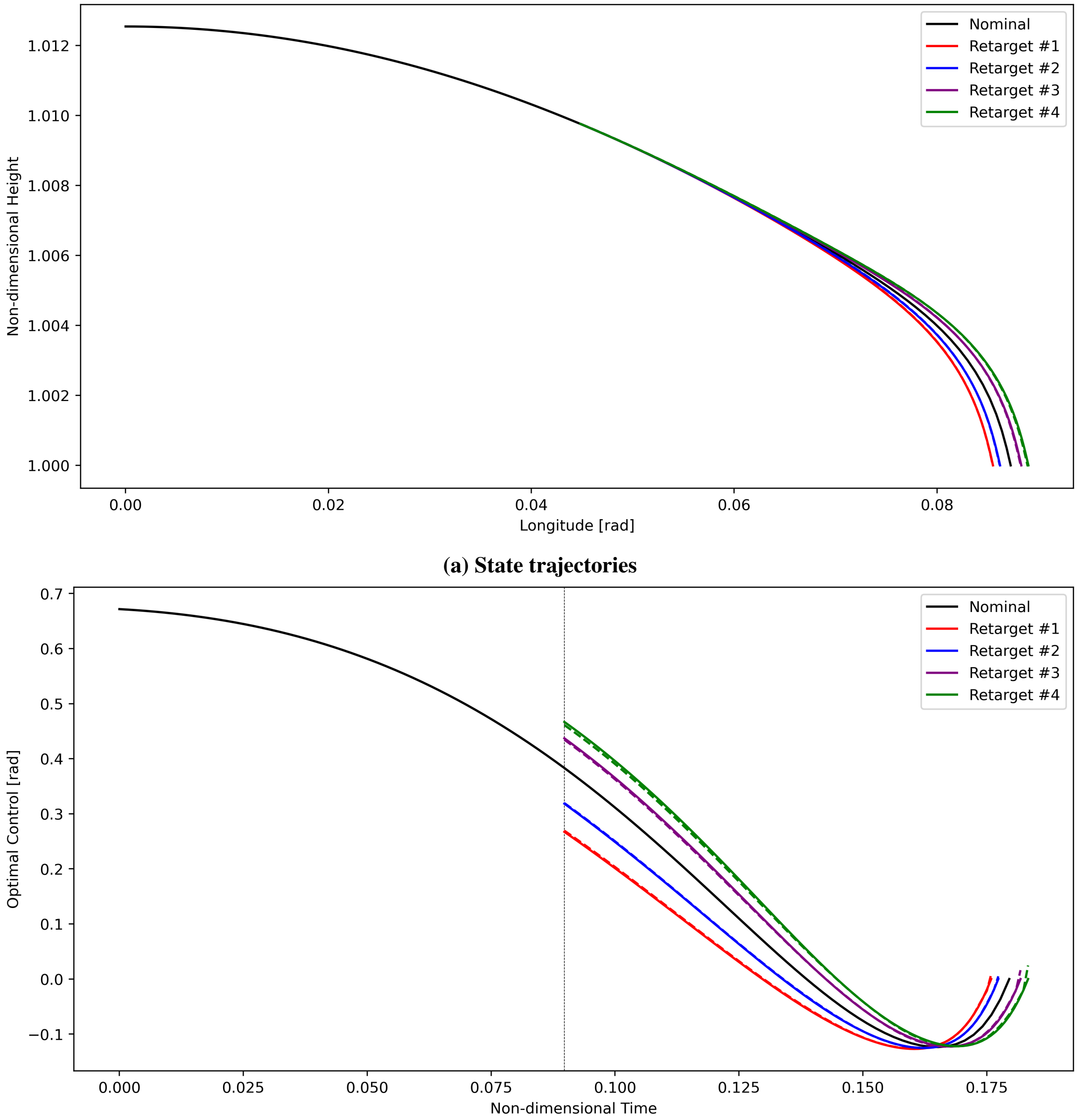

(a) State trajectories

(b) Optimal control trajectories

Figure 10 State and optimal control trajectories obtained from the open-loop continuation method and the feedback controller for the re-targeting scenario at 50% of the nominal trajectory. Solid: open-loop solution. Dashed: feedback controller solution.

Table 6 Accuracy of the feedback controller for ten different test re-target points at 50% of the nominal trajectory.

Variable	**Mean Least-squares RMSE**	**Mean Sparse RMSE**
Altitude: h	8.297×10^{-6}	7.344×10^{-6}
Velocity: v	6.322×10^{-4}	6.233×10^{-4}
Flight-path Angle: γ	2.890×10^{-3}	1.935×10^{-4}
Longitude: θ	1.356×10^{-5}	1.301×10^{-5}
Costate: λ_v	3.283×10^{-3}	5.067×10^{-3}
Costate: λ_γ	9.467×10^{-4}	7.048×10^{-4}
Optimal Control: u^*	2.021×10^{-3}	1.728×10^{-3}

The re-targeting results at 20% and 50% of the nominal trajectory demonstrate the accuracy of the feedback controller in generating real-time optimal control. Furthermore, these results demonstrate that the sparse optimization algorithm effectively selects the necessary number of basis functions that yield sparse functional approximations with an accuracy comparable to the non-sparse least-squares solution, and that is less prone to overfitting.

V. Conclusion

A data-driven framework for generating optimal feedback controllers is presented in this paper that addresses re-targeting problems for hypersonic trajectories. The framework is suitable for problems that include initial and terminal state uncertainties, and enables rapid and highly accurate estimates of the optimal control to reach any re-target point once the hypersonic vehicle has been deployed in a nominal trajectory.

Given initial and terminal condition uncertainties, the Conjugate Unscented Transformation (CUT) algorithm is utilized to efficiently sample the mission parameter space. Indirect optimal control in conjunction with a numerically robust two-point boundary value problem solver such as stabilized continuation are used to generate a dataset of open-loop trajectories. Consequently, Hamilton-Jacobi-Bellman theory along with a sparse learning optimization framework is adopted to identify a sparse approximation to the solution of the HJB equation using the dataset of open-loop trajectories. This approximate HJB solution along with the stationarity condition from indirect optimal control enable the computation of the optimal control for any given state of the hypersonic vehicle.

The end-result optimal feedback controller is utilized to generate nominal and re-targeting hypersonic trajectories that are ensured to be close to optimal. The resulting states, costates, and controls produced by the feedback controller are demonstrated to accurately replicate the open-loop trajectories obtained from the stabilized continuation method. These results effectively render the feedback controller suitable for rapid optimal trajectory generation for missions with presence of uncertainty in the deployment and terminal states.

References

[1] Schierman, J., and Hull, J., "In-flight entry trajectory optimization for reusable launch vehicles," *AIAA guidance, navigation, and control conference and exhibit*, 2005, p. 6434.

[2] Sagliano, M., Mooij, E., and Theil, S., "Onboard trajectory generation for entry vehicles via adaptive multivariate pseudospectral interpolation," *Journal of Guidance, Control, and Dynamics*, Vol. 40, No. 2, 2016, pp. 466–476.

[3] Gaudet, B., Linares, R., and Furfaro, R., "Integrated Guidance and Control for Pinpoint Mars Landing Using Reinforcement Learning," *AAS/AIAA Astrodynamics Specialist Conference*, 2018, pp. 1–20.

[4] Chai, R., Tsourdos, A., Savvaris, A., Chai, S., Xia, Y., and Chen, C. P., "Six-DOF Spacecraft Optimal Trajectory Planning and Real-Time Attitude Control: A Deep Neural Network-Based Approach," *IEEE Transactions on Neural Networks and Learning Systems*, 2019.

[5] Fahroo, F., and Ross, I. M., "Direct trajectory optimization by a Chebyshev pseudospectral method," *Journal of Guidance, Control, and Dynamics*, Vol. 25, No. 1, 2002, pp. 160–166.

[6] Fahroo, F., and Doman, D., "A direct method for approach and landing trajectory reshaping with failure effect estimation," *AIAA Guidance, Navigation, and Control Conference and Exhibit*, 2004, p. 4772.

[7] Gill, P. E., Murray, W., and Saunders, M. A., "SNOPT: An SQP algorithm for large-scale constrained optimization," *SIAM Rev.*, Vol. 47, 2005, pp. 99–131.

[8] Schlueter, M., Erb, S. O., Gerdts, M., Kemble, S., and Rückmann, J.-J., "MIDACO on MINLP space applications," *Advances in Space Research*, Vol. 51, No. 7, 2013, pp. 1116–1131.

[9] Wei, X., Liu, L., Wang, Y., and Yang, Y., "Reentry Trajectory Optimization for a Hypersonic Vehicle Based on an Improved Adaptive Fireworks Algorithm," *International Journal of Aerospace Engineering*, Vol. 2018, 2018.

[10] Li, Z., Hu, C., Ding, C., Liu, G., and He, B., "Stochastic gradient particle swarm optimization based entry trajectory rapid planning for hypersonic glide vehicles," *Aerospace Science and Technology*, Vol. 76, 2018, pp. 176–186.

[11] Bryson, A. E., *Applied optimal control: optimization, estimation and control*, CRC Press, 1975, Chap. Optimization problems for dynamic systems, pp. 42–87.

[12] Allgower, E. L., and Georg, K., *Introduction to numerical continuation methods*, SIAM, 2003, pp. 7–15.

[13] Grant, M., Clark, I., and Braun, R., "Rapid simultaneous hypersonic aerodynamic and trajectory optimization using variational methods," *AIAA Atmospheric Flight Mechanics Conference*, 2011, p. 6640.

[14] Grant, M. J., and Braun, R. D., “Rapid indirect trajectory optimization for conceptual design of hypersonic missions,” *Journal of Spacecraft and Rockets*, Vol. 52, No. 1, 2014, pp. 177–182.

[15] Grant, M. J., and Antony, T., “Rapid indirect trajectory optimization of a hypothetical long range weapon system,” *AIAA Atmospheric Flight Mechanics Conference*, 2016, p. 0276.

[16] Mall, K., and Taheri, E., “Unified Trigonometrization Method for Solving Optimal Control Problems in Atmospheric Flight Mechanics,” *AIAA Scitech 2020 Forum*, 2020, p. 0022.

[17] Saranathan, H., and Grant, M. J., “Relaxed Autonomously Switched Hybrid System Approach to Indirect Multiphase Aerospace Trajectory Optimization,” *Journal of Spacecraft and Rockets*, Vol. 55, No. 3, 2017, pp. 611–621.

[18] Ohtsuka, T., and Fujii, H., “Stabilized continuation method for solving optimal control problems,” *Journal of Guidance, Control, and Dynamics*, Vol. 17, No. 5, 1994, pp. 950–957.

[19] Kotamraju, G. R., and Akella, M. R., “Stabilized continuation methods for boundary value problems,” *Applied Mathematics and Computation*, Vol. 112, No. 2-3, 2000, pp. 317–332.

[20] Vedantam, M., Akella, M. R., and Grant, M. J., “Multi-Stage Stabilized Continuation for Indirect Optimal Control of Hypersonic Trajectories,” *AIAA Scitech 2020 Forum*, 2020, p. 0472.

[21] Vedantam, M., Akella, M. R., and Grant, M. J., “Jacobian Conditioned Two-Layer Stabilized Continuation for Computing Optimal Hypersonic Trajectories,” *AIAA SCITECH 2022 Forum*, 2022, p. 1890.

[22] Adurthi, N., Singla, P., and Majji, M., “Sparse approximation-based collocation scheme for nonlinear optimal feedback control design,” *Journal of Guidance, Control, and Dynamics*, Vol. 40, No. 2, 2017, pp. 248–264.

[23] Mercurio, M., Adurthi, N., Singla, P., and Majji, M., “A collocation-based approach to solve the finite horizon hamilton-jacobi-bellman equation,” *2016 American Control Conference (ACC)*, IEEE, 2016, pp. 3322–3327.

[24] Mercurio, M., “Sparse Collocation Methods for Solving High Dimension PDES in Estimation and Control of Dynamical Systems,” Ph.D. thesis, State University of New York at Buffalo, 2017.

[25] Mercurio, M., Singla, P., and Majji, M., “A Conjugate Unscented Transform-Based Scheme for Optimal Control with Terminal State Constraints,” *2018 Annual American Control Conference (ACC)*, IEEE, 2018, pp. 2651–2656.

[26] Adurthi, N., Singla, P., and Singh, T., “Conjugate unscented transformation: Applications to estimation and control,” *Journal of Dynamic Systems, Measurement, and Control*, Vol. 140, No. 3, 2018.

[27] Boyd, S., and Vandenberghe, L., *Convex Optimization*, Cambridge University Press, 2004, pp. 127–188.

[28] Grant, M., and Boyd, S., “CVX: Matlab Software for Disciplined Convex Programming, version 2.1,” `http://cvxr.com/cvx`, Mar. 2014.